

# Methylcyclohexane transformation over H-EU-1 zeolite: Selectivity and catalytic role of the acid sites located at the pore mouths

P.C. Mihindou-Koumba, J.-D. Comparot, S. Laforge\*, P. Magnoux

*Laboratoire de Catalyse en Chimie Organique, UMR 6503 CNRS–Université de Poitiers, 40 avenue du Recteur Pineau, 86022 Poitiers Cedex, France*

Received 3 December 2007; revised 27 February 2008; accepted 27 February 2008

Available online 21 March 2008

## Abstract

The catalytic transformation of methylcyclohexane (mcha), as representative of the reactions taking place during catalytic cracking, was carried out on a H-EU-1 zeolite under the following conditions: 623 K, atmospheric pressure,  $p_{N_2}/p_{mcha}$  ratio equal to 9, contact time (taken as the reciprocal of the weight hourly space velocity) between 0.016 and 0.3 h. Whatever the contact time and time-on-stream, cracking was the main reaction, like on other 10-MR zeolites, but significant amounts of isomers and aromatics were produced. Moreover, cracking led predominantly to branched products, in contradiction with the shape selectivity expected from the narrow pore openings of this 10-MR zeolite. All this could be explained by a very important catalytic contribution of the protonic sites located at the pore mouths. Additional experiments using bulky basic compounds ( $\gamma$ -collidine) confirmed this hypothesis and allowed estimation of the selectivity of these acid sites.

© 2008 Elsevier Inc. All rights reserved.

**Keywords:** H-EU-1 zeolite; Cracking; Methylcyclohexane; Deactivation; Coke; Active sites; Pore mouth

## 1. Introduction

Fluid catalytic cracking (FCC) is an important process in refining, both in terms of feedstock and catalyst amounts [1–3]. This process consists in a fragmentation of the heavy oil cuts (boiling point > 523 K) into smaller hydrocarbons, using a solid acid catalyst, at a temperature close to 773 K and atmospheric pressure. The typical feedstock used in the FCC unit is vacuum gas oil (VGO), whose transformation gives a wide range of products, ranging from light gases ( $H_2$  and  $C_1$ – $C_4$  hydrocarbons) to heavy products (high cycle oil and slurry).

Vacuum gas oil is mainly composed of naphthenes, aromatics and alkanes. Whereas transformations of alkanes and aromatics have been studied extensively, only a few publications have been devoted to naphthene's transformation. Even so, this transformation, and in particular methylcyclohexane transformation, involves all of the reactions taking place during VGO conversion: isomerization, cracking, hydrogen transfer (aromatization), and coking [4–6]. Therefore, although the

methylcyclohexane transformation is complex, it can be used as a model reaction to evaluate catalyst performance and to characterize both acidity and porosity of zeolites. The following observations can be drawn from the few publications devoted to this reaction. First, global activity is largely dependent on the reaction temperature, but also depends on the acid strength of the active sites; the higher the concentration in strong protonic sites (and the temperature), the higher the activity (and the deactivation) [4,6].

Second, the distribution of products is largely dependent on the pore architecture. Thus, the combination of large pore openings and large cages of H-FAU zeolites leads to an important formation of isomers [6–8], whereas this formation is lower in the tridimensional channel system of H-BEA zeolites, likely due to a longer residence time of these isomers inside the H-BEA pores, which leads to their substantial cracking [7,9]. Moreover, in the medium-pore size H-MFI zeolite, isomers are formed in a very low amount, cracking being the main reaction [6,10].

Finally, coke formation during methylcyclohexane transformation at 723 K depends largely on the nature of the zeolite.

\* Corresponding author. Fax: +33 (0) 5 49 45 37 79.

E-mail address: [sebastien.laforge@univ-poitiers.fr](mailto:sebastien.laforge@univ-poitiers.fr) (S. Laforge).

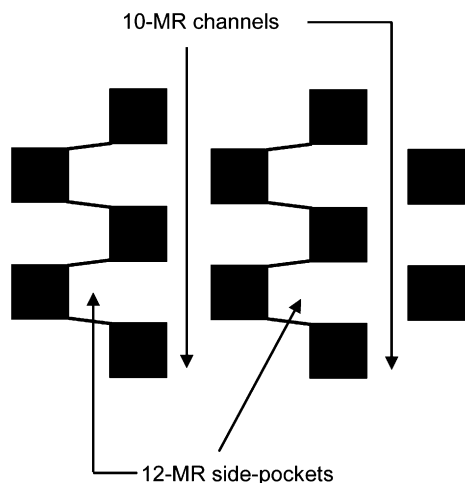


Fig. 1. Schematic representation of the EUO zeolite pore system.

It is faster and more significant in large-pore zeolites (H-FAU, H-BEA) [8,9,11] than in medium-pore zeolites (H-MFI) [10].

In this paper, the methylcyclohexane transformation at 723 K is used to investigate the catalytic properties of H-EU-1 zeolite [12], a relatively recent medium-pore zeolite, which belongs to the EUO framework type [13]. The pore architecture of this zeolite is formed by a monodimensional system of 10-membered ring (10-MR) channels ( $0.58 \times 0.41$  nm), along which wide 12-MR pockets (cross-section of  $0.68 \times 0.58$  nm; 0.8 nm depth) are alternatively disposed [14]. A schematic representation of EUO zeolite framework structure is shown in Fig. 1. The coexistence of narrow channels and wide pockets imparts very interesting catalytic properties to EUO-type zeolites, which are intermediate between those of large-pore zeolites and medium-pore size zeolites [15–18].

The most interesting results concern the isomerization of the  $C_8$ -aromatic cut [19–21]. Thus, during ethylbenzene transformation on Pt/Al<sub>2</sub>O<sub>3</sub>–H-EU-1 catalysts, the initial selectivity is that of a 10-MR zeolite (ZSM-5; low selectivity toward isomerization) whereas at long time on stream, the selectivity is similar to that of a 12-MR zeolite (MOR, highly selective for isomerization) [22]. This change in selectivity is accompanied by a strong deactivation of the catalyst, due to a complete blockage of the access to the 10-MR channels (and side pockets) by coke molecules. Therefore, the remaining catalytic activity should be ascribed to the acid sites of side pockets located on the external surface of the EUO crystallites [13], which would be very selective toward isomerization. Due to the small depth of these pockets (0.8 nm), these acid sites would be very close to the pore mouths, and thus the catalytic behavior of the EUO zeolite can be considered as a new example of “pore mouth catalysis.” Martens et al. [23,24] first introduced this concept to explain the particular behavior of ZSM-22 zeolites during the hydrocracking of long-chain *n*-alkanes. The determination of the location of the active sites and of the potential contribution of the “external” acid sites during methylcyclohexane transformation on EUO-type zeolites is one objective of the present investigation.

## 2. Experimental

### 2.1. Materials

The EU-1 zeolite (total Si/Al ratio of 15) used in this work was provided by IFP. Its synthesis procedure was derived from Ref. [12] (example 1), using 1,6-*N,N,N',N',N'*-hexamethylhexamethylene diammonium dibromide (hexamethonium bromide) as a template. First, 60 g of colloidal silica (Ludox AS40, Dupont, 40 wt% SiO<sub>2</sub>) were added to a mixture of 257 g of water and 47.1 g of template (Fluka, >95%). Subsequently, 6.12 g of sodium hydroxide (Prolabo, 99%) and 2.22 g of sodium aluminate (Prolabo, 46 wt% Al<sub>2</sub>O<sub>3</sub>, 33 wt% Na<sub>2</sub>O) were dissolved in 35 g of water and combined with the silica–template mixture. The resulting slurry was then reacted in a stainless steel autoclave under stirring at 300 rpm for 5 days at 453 K under autogeneous pressure. After cooling at room temperature, the solid product was filtered and washed with 300 mL of demineralized water and then dried in a ventilated oven at 393 K.

To remove the template, the as-synthesized zeolite was calcined in air flow ( $1 \text{ L h}^{-1} \text{ g}^{-1}$ ) using the following temperature program: 1 h at 423, 523, 623, 723 and 823 K (heating rates of  $1 \text{ K min}^{-1}$ ). The resulting material (Na,H-EU-1) was then thrice exchanged with a 1 M ammonium nitrate solution, in reflux, under vigorous stirring for 4 h. Each exchange step was followed by filtration, washing with demineralized water, and drying at 373 K for 12 h. The protonic form of the zeolite (H-EU-1) was then obtained by calcination of the exchanged zeolite under air flow at 823 K for 4 h.

### 2.2. Nitrogen adsorption

The porosity characteristics of the zeolite samples were determined by nitrogen adsorption at 77 K, using a Micromeritics ASAP 2000 apparatus. Before adsorption, the zeolite samples were degassed in vacuum at 363 K for 1 h and then 623 K for 12 h (fresh samples) or 473 K for 1 h (coked samples). The total pore volume ( $V_{\text{total}}$ ) was calculated from the adsorbed volume of nitrogen for a relative pressure  $P/P_0$  of 0.97, whereas the ultramicropore volume ( $V_{\text{ultra}}$ , micropores with a diameter <0.8 nm), and the external surface area were determined by using the *t*-plot method [25,26]. The supermicropore volume ( $V_{\text{super}}$ , micropores with diameters of 0.8–2.0 nm) was determined by difference between the total micropore volume estimated from the Dubinin–Raduskevitch equation ( $V_{\text{DR}}$ ) [25] and  $V_{\text{ultra}}$  and the mesopore volume was given by the difference  $V_{\text{total}} - V_{\text{DR}}$ .

### 2.3. IR experiments

The acidic properties of the zeolite samples were characterized by adsorption of two basic probe molecules (pyridine and 2,4-dimethylquinoline), followed by infrared (IR) spectroscopy. IR spectra were recorded with a Nicolet NEXUS FTIR spectrometer, in a quartz IR cell connected to a vacuum line. Before measurements, thin self-supported wafers of the

zeolite (8–15 mg) were activated in the IR cell at 723 K for 12 h under air flow ( $60 \text{ mL min}^{-1}$ ) and then at 473 K for 1 h under vacuum ( $10^{-3} \text{ Pa}$ ). The IR spectrum of the “fresh” sample was recorded at room temperature after this pretreatment. For “coked” samples, activation involved only evacuation under vacuum at 423 K for 1 h.

Pyridine vapor was introduced in excess (2–3 mbar) in the IR cell at 423 K and adsorbed onto the activated zeolite. After outgassing at the same temperature ( $10^{-3} \text{ Pa}$ , 1 h) to eliminate the physisorbed molecules, a spectrum was recorded, and the total concentrations of Brønsted and Lewis acid sites were calculated from the area of the bands at 1545 (pyridinium ions) and  $1455 \text{ cm}^{-1}$  (pyridine coordinated to Lewis sites), respectively, using the extinction coefficients determined previously [27]. To evaluate the strength of the zeolite acid sites, desorption of pyridine was performed in vacuum over four consecutive 1-h periods of heating at 523, 623, 723, and 773 K, each followed by an IR measurement at room temperature.

Because 2,4-dimethylquinoline (2,4-DMQ) is not sufficiently volatile for introduction in the gas phase, 2,4-DMQ (Aldrich, >97%) was solubilized in methylene chloride (20–40  $\mu\text{mol}$  per 1 mL of solvent), and the solution was deposited homogeneously on the surface of the pretreated zeolite wafer. Then the solvent was evacuated in vacuum (393 K), and IR spectra of adsorbed 2,4-DMQ were recorded. The temperature was then increased without evacuation (closed cell). After 20 min at 473 K (and then 573 K), the sample was evacuated in vacuum, and IR spectra were recorded. The concentrations of quinolinium ions were calculated from the area of the band at  $1648 \text{ cm}^{-1}$ , using the extinction coefficients determined previously [28].

#### 2.4. Methylcyclohexane transformation

The transformation of methylcyclohexane (Aldrich, >99%) was performed in a fixed-bed reactor at 623 K and under atmospheric pressure, with nitrogen as a carrier gas ( $p_{\text{N}_2}/p_{\text{mcha}} = 9$ ). Different values of the contact time  $\tau$  (taken as the reciprocal of the weight hourly space velocity) were obtained by varying the mass of the catalyst (30–300 mg) and/or the reactant flow ( $1.33\text{--}6 \text{ mL h}^{-1}$ ). For the catalytic tests, the zeolite was used in the form of pellets, sieved at 0.2–0.4 mm. Before reaction, the zeolite was activated in situ at 723 K overnight under air flow ( $60 \text{ mL min}^{-1}$ ), and then cooled to the reaction temperature under nitrogen. The reaction products were analyzed online by FID gas chromatography using a 50-m plot  $\text{Al}_2\text{O}_3/\text{KCl}$  fused silica capillary column.

The poisoning experiments were performed by adding 15  $\mu\text{L}$  of  $\gamma$ -collidine (2,4,6-trimethylpyridine, Fluka, >99%) in 10 mL of methylcyclohexane. Under the operating conditions (100 mg of zeolite and  $4 \text{ mL h}^{-1}$  of methylcyclohexane), this corresponds to the addition of  $450 \mu\text{mol g}_{\text{zeo}}^{-1}$  of collidine after 60 min of reaction, that is, approximately 80% of the total concentration of protonic sites.

Table 1  
Textural characteristics of the H-EU-1 sample

$V_{\text{total}}$ ( $\text{cm}^3 \text{ g}^{-1}$ )	$V_{\text{ultramicro}}$ ( $\text{cm}^3 \text{ g}^{-1}$ )	$V_{\text{supermicro}}$ ( $\text{cm}^3 \text{ g}^{-1}$ )	$V_{\text{meso}}$ ( $\text{cm}^3 \text{ g}^{-1}$ )	$S_{\text{ext}}$ ( $\text{m}^2 \text{ g}^{-1}$ )
0.268	0.139	0.018	0.111	50.6

Note.  $V_{\text{total}}$  = total pore volume (at  $P/P_0 = 0.97$ );  $V_{\text{ultramicro}}$  = ultramicro-pore volume;  $V_{\text{supermicro}}$  = supermicropore volume;  $V_{\text{meso}}$  = mesopore volume.

#### 2.5. Coke analysis

After reaction, the carbon content of the coked zeolites was determined by total burning at 1293 K under helium and oxygen in a Thermoquest NA2100 analyzer. The coke components were identified using the method developed in our laboratory [29,30]. The zeolite was dissolved in a hydrofluoric acid solution (40%), after which the soluble part of the carbonaceous compounds was recovered with a methylene chloride/*n*-pentane mixture (1/1) and analyzed with a GC/MS spectrometer (Automass Multi Thermoelectron).

### 3. Results and discussion

#### 3.1. Characterization of the H-EU-1 sample

The textural characteristics of the H-EU-1 sample are summarized in Table 1. Scanning electron microscopy photographs of the sample and nitrogen adsorption isotherm (at 77 K) can be found in Ref. [22]. The sample exhibited the usual “rice grain” shape of EU-1 zeolites and was formed by agglomerates of very small crystallites (ca. 50 nm). The nitrogen adsorption isotherm exhibited the characteristics of a type I-b isotherm in the IUPAC classification [31]. Due to the very small size of the zeolite crystallites, the mesopores and supermicropores most likely were interparticular.

The IR spectra of the H-EU-1 sample before and after pyridine adsorption at 423 K followed by evacuation at increasing temperature are shown in Fig. 2. The IR spectrum of the fresh sample, in the hydroxyl stretching region (Fig. 2A, spectrum a), exhibited the following bands:

- An intense band at  $3745 \text{ cm}^{-1}$  with a shoulder at ca.  $3730 \text{ cm}^{-1}$ , respectively attributed to external and internal silanol groups.
- A broad band at  $3660 \text{ cm}^{-1}$  of low intensity, corresponding to hydroxyl groups linked to extra-framework aluminum species (EFAI), likely formed during calcination or cationic exchange.
- An intense band centered at  $3605 \text{ cm}^{-1}$ , attributed to bridging hydroxyl groups Si(OH)Al.

The addition of pyridine at 423 K followed by its evacuation in vacuum at the same temperature led to the quasi-complete disappearance of the band at  $3605 \text{ cm}^{-1}$  and a slight reduction in the intensity of the other OH bands (Fig. 2A, spectrum b). At the same time, the bands characteristic of pyridine adsorbed on Brønsted or Lewis acidic species were observed in the 1400–

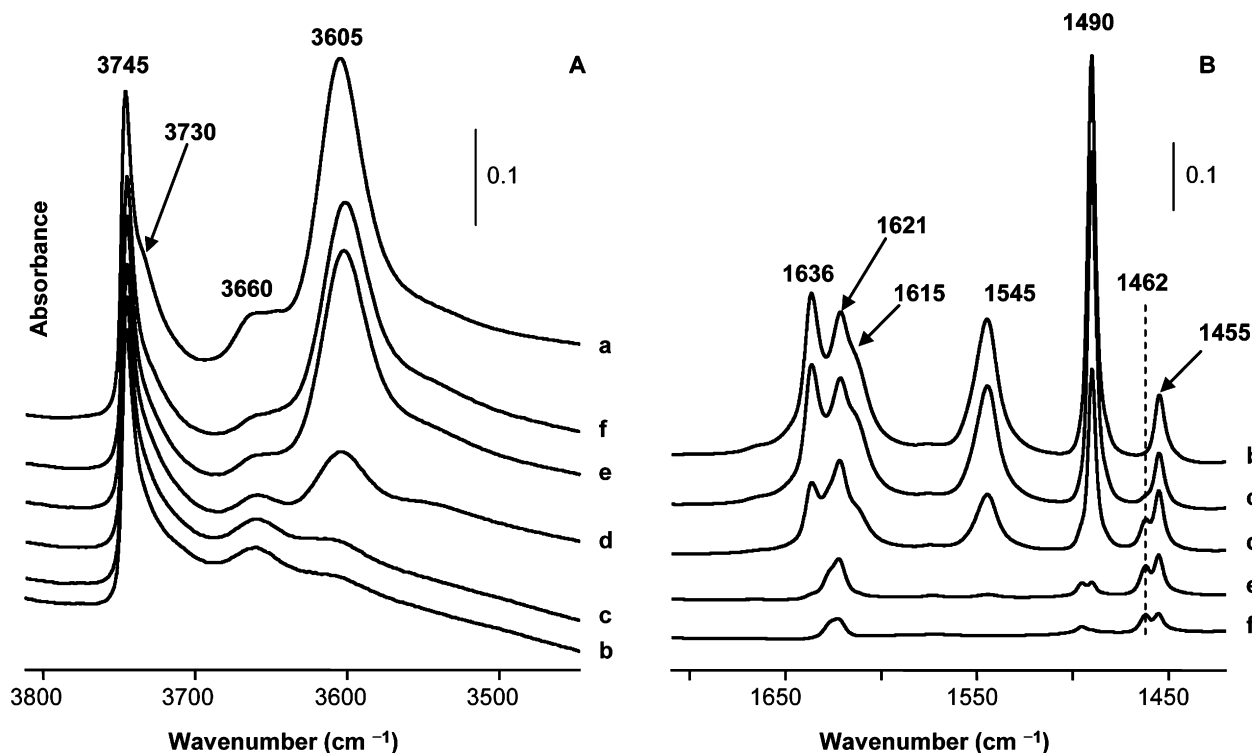


Fig. 2. IR spectra of the H-EU-1 sample before (a) and after pyridine adsorption at 423 K followed by desorption in vacuum at 423 K (b), 523 K (c), 623 K (d), 723 K (e) and 773 K (f). (A) Spectra obtained in the  $\nu(\text{OH})$  region. (B) Difference spectra (spectrum obtained after pyridine evacuation at a given temperature—spectrum obtained before pyridine adsorption) in the  $\nu(\text{CC})$  and  $\nu(\text{CN})$  region.

Table 2  
Acid sites concentrations (in  $\mu\text{mol g}^{-1}$ ) calculated from adsorption/desorption of various probe molecules followed by infrared spectroscopy

Theo <sup>a</sup>	Pyridine (Brönsted/Lewis sites) <sup>b</sup>		2,4-DMQ <sup>b</sup>
	423 K	723 K	
950	553/118	9/74	56

<sup>a</sup> Theoretical acid sites concentration (Theo) was estimated from the sample cell formula.

<sup>b</sup> Pyridine was adsorbed at 423 K and then evacuated at 423 or 723 K; 2,4-dimethylquinoline (2,4-DMQ) was adsorbed at room temperature and then evacuated at 473 K.

1700  $\text{cm}^{-1}$  region (Fig. 2B, spectrum b). The bands at 1490, 1545, and 1636  $\text{cm}^{-1}$  are related to the pyridinium ion (pyridine adsorbed on Brönsted acid site), whereas those at 1455, 1490, and 1621  $\text{cm}^{-1}$  are characteristic of pyridine coordinated to Lewis acid sites [32,33]. Consequently, the total concentrations of Brönsted (protonic) and Lewis acid sites can be estimated, using the area of the bands at 1545 and 1455  $\text{cm}^{-1}$ , respectively, and the extinction coefficients determined previously in our laboratory [27]. The values thus obtained are reported in Table 2.

The total concentration of acid sites obtained by pyridine adsorption (Brönsted + Lewis) was low ( $671 \mu\text{mol g}^{-1}$ ) compared with that calculated from the zeolite cell formula (Theo,  $950 \mu\text{mol g}^{-1}$ ). This difference can be explained in part by the fact that pyridine adsorption did not lead to a complete disappearance of the bands at 3660 and 3605  $\text{cm}^{-1}$ , attributed to hydroxyl groups linked to EFAl species and bridging hy-

droxyl groups, respectively (spectrum b in Fig. 2A). This could have resulted from either the very low acidity of these hydroxyl groups (which were insufficiently acidic to retain pyridine adsorbed even at 423 K) or the inaccessibility to a small fraction of these hydroxyl groups, due to pore blockage by EFAl. Another possible cause could be the extraction of aluminum from the zeolite framework, leading to the formation of EFAl, as demonstrated by the presence of Lewis acid sites as well as by the appearance of the band at 3660  $\text{cm}^{-1}$ , related to hydroxyl groups linked to EFAl. This band was slightly affected by pyridine adsorption, indicating that most of these hydroxyl groups were probably not acidic. Moreover, the small decrease in the bands at 3745 and 3730  $\text{cm}^{-1}$  (attributed to silanol groups) suggests that a small part of these species interacted with pyridine, most likely through hydrogen bonding.

It is generally admitted that the temperature required to desorb pyridine from a given acid site can be correlated to the acid strength of this site; the higher the temperature, the stronger the site. The IR spectra obtained after pyridine adsorption at 423 K, followed by evacuation at 423, 523, 623, 723 and 773 K, are given in Figs. 2A and 2B (spectra b, c, d, e and f, respectively). As expected, the increase in evacuation temperature from 423 to 773 K is followed by a progressive reconstruction of the bands in the 3500–3800  $\text{cm}^{-1}$  region (Fig. 2A) and a progressive disappearance of the bands corresponding to adsorbed pyridine in the 1400–1700  $\text{cm}^{-1}$  region (Fig. 2B). Three observations are made. First, when the evacuation temperature was raised, pyridine desorption was not accompanied by a total reconstruction of the hydroxyl bands, even at 773 K



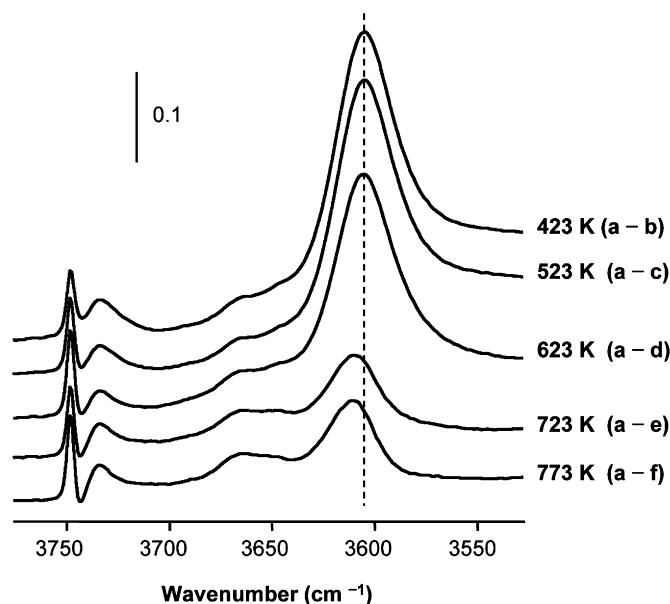


Fig. 3. Evolution of the bands corresponding to the hydroxyl groups interacting with pyridine, for different values of the evacuation temperature. The spectra presented in this figure were obtained by difference between spectrum a and spectra b, c, d, e or f in Fig. 2A.

(Fig. 2A, spectrum f), whereas the bands attributed to pyridinium ions were completely suppressed when the temperature reached 773 K (Fig. 2B, spectrum f). This is confirmed by the difference spectra shown in Fig. 3, which were obtained by the difference between the spectrum of the fresh zeolite (Fig. 2A, spectrum a) and the spectra obtained after pyridine adsorption and evacuation at different temperatures (Fig. 2A, spectra b, c, d, e and f). Thus, they correspond to the OH groups still interacting with pyridine after evacuation at a given temperature. It is generally accepted that the acid sites able to retain pyridine at a temperature higher than 623 K can be considered strong acid sites. But in this case, a small part of the silanol groups and of the OH groups linked to EFAl, as well as a significant fraction of the bridging hydroxyl groups, would be strong acid sites. This is quite surprising in the case of the silanol groups, which are usually considered as very weak acid sites. In fact, comparing Figs. 2A and 3 suggests that the fraction of external silanol groups ( $3745\text{ cm}^{-1}$ ) interacting with pyridine is very small, whereas the fraction of internal silanol groups ( $3730\text{ cm}^{-1}$ ) interacting with pyridine seems to be very significant. It is generally known that these silanol groups are located at defects created by dealumination of the zeolite framework and thus probably close to Lewis acid sites. Therefore, if their interaction with pyridine occurs with a pyridine molecule adsorbed on a Lewis acid site, then the persistence of this interaction at high temperature could be explained by the strength of the Lewis acid sites; most of them (63%, according to the area of the band at  $1455\text{ cm}^{-1}$ ) were able to retain pyridine at 723 K.

Second, the increase of pyridine evacuation temperature leads to the appearance of a new band at  $1462\text{ cm}^{-1}$  (Fig. 2B). This band can be attributed to the formation of iminium ions [34,35]. According to Chiche et al. [35], these iminium ions would be formed at high temperature by interaction of a pyrid-

inium ion with a Lewis acid site. This interaction may explain why some of the hydroxyl groups, particularly the bridging hydroxyl groups, are not recovered after pyridine evacuation at 723 and 773 K. The areas of the bands at  $1545$  and  $1455\text{ cm}^{-1}$  in the spectrum obtained after pyridine evacuation at 723 K (Fig. 2B, spectrum e), were used to estimate the respective concentrations of strong Brønsted (protonic) and Lewis acid sites. The values obtained, given in Table 2, demonstrate that the H-EU-1 sample contains only a small fraction of strong protonic sites ( $9\text{ }\mu\text{mol g}^{-1}$ , corresponding to  $<2\%$  of the total concentration).

Third, Fig. 3 shows that the maximum of the band at around  $3605\text{ cm}^{-1}$  (corresponding to the bridging hydroxyl groups interacting with pyridine) progressively shifted to higher frequencies with increasing evacuation temperature increases. This suggests that the band centered at  $3605\text{ cm}^{-1}$  was composed of several components. According to other authors who examined the IR spectra of mordenite [36,37], two bands should exist: one at high wavenumber, corresponding to bridging hydroxyl groups located in the 12-MR side pockets, and a second at lower wavenumber, corresponding to bridging hydroxyl groups located in the 10-MR channels. The shift in the maximum of the band with increasing evacuation temperature indicates that the bridging hydroxyl groups able to retain pyridine at high temperature (hence those with the strongest acidity) were located mainly inside the 12-MR side pockets.

The concentration of external protonic sites was estimated by 2,4-dimethylquinoline (2,4-DMQ) adsorption. This compound was demonstrated to be too bulky to enter the pores of medium-pore size zeolites, such as MFI [38] or MWW [28], and thus would adsorb only on protonic sites located on the external surface of zeolite crystallites. The IR spectra of the H-EU-1 zeolite before and after adsorption of 2,4-DMQ at room temperature followed by evacuation at 473 and 573 K are given in Fig. 4. This figure shows that adsorption of 2,4-DMQ led to a partial decrease in the bands at  $3745$  and  $3605\text{ cm}^{-1}$ , along with appearance of a band at  $3733\text{ cm}^{-1}$ . When the evacuation temperature of 2,4-DMQ was raised from 473 to 573 K, the band at  $3745\text{ cm}^{-1}$  was partially rebuilt, and the band at  $3733\text{ cm}^{-1}$  was diminished. Based on, this last band can be plausibly attributed to silanol groups interacting weakly with 2,4-DMQ, probably through hydrogen bonding [22]. On the other hand, the evacuation temperature had no effect on the decrease of the Si(OH)Al band, at  $3605\text{ cm}^{-1}$ , suggesting a stronger interaction of these sites with 2,4-DMQ molecules. Therefore, the presence of a band at  $1649\text{ cm}^{-1}$  in both spectra recorded after 2,4-DMQ adsorption (not shown here) indicates the formation of protonated 2,4-DMQ molecules (quinolinium ions) [28,38]. Like the band at  $3605\text{ cm}^{-1}$ , this band was not affected by the increase in evacuation temperature, suggesting a relationship between the decrease in Si(OH)Al and the formation of quinolinium ions. Moreover, the quinolinium ion concentration, estimated using the extinction coefficient previously published [28], was  $56\text{ mmol g}^{-1}$  (Table 2), representing 10% of the total protonic site concentration estimated from pyridine adsorption. This percentage is close to that obtained from the decrease of the band at  $3605\text{ cm}^{-1}$  (12%), suggesting that the quinolinium ions are

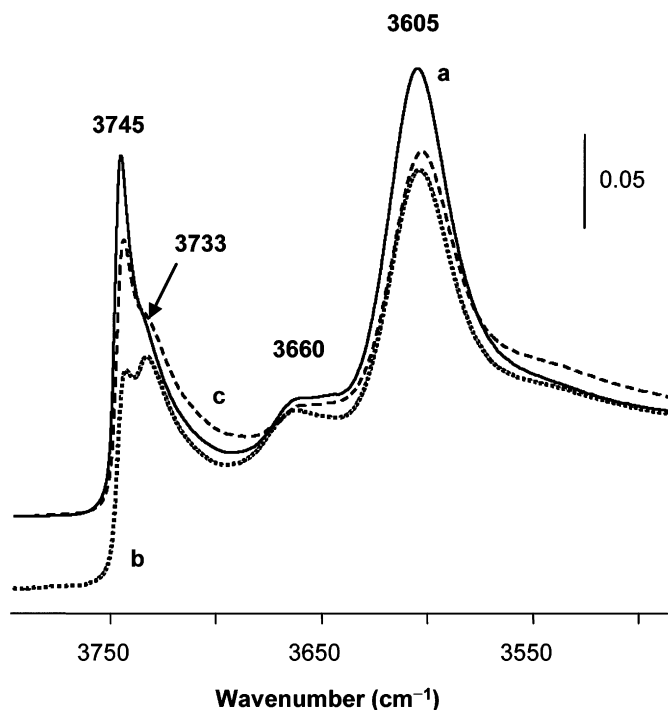


Fig. 4. Adsorption of 2,4-dimethylquinoline (2,4-DMQ). IR spectra obtained on the activated EU-1 sample (a) and after 2,4-DMQ adsorption at 473 K followed by evacuation in vacuum at 473 K (b) or 573 K (c).

(mostly) formed on bridging hydroxyl groups, probably located at the pore mouths, not on the external surface of the zeolite crystallites. Indeed, previous studies on MWW family materials have shown that acidic OH groups located on the external surface of zeolite crystallites do not give rise to a detectable IR band, and that their interaction with 2,4-DMQ molecules does not lead to a significant decrease in the IR band associated with bridging hydroxyl groups [28,39].

### 3.2. Methylcyclohexane transformation on H-EU-1 zeolite

#### 3.2.1. Transformation on fresh zeolite

The products obtained during methylcyclohexane transformation were those typically reported in the literature [4–11]:

- Methane, formed through protolytic cracking of methylcyclohexane.
- C<sub>2</sub>–C<sub>7</sub> alkenes, resulting from methylcyclohexane cracking;
- Dimethylcyclopentanes, formed through methylcyclohexane isomerization.
- Benzene and higher aromatics (xylenes, trimethylbenzenes), resulting from methylcyclohexane aromatization and toluene secondary transformations.
- C<sub>2</sub>–C<sub>7</sub> alkanes, formed by hydrogen transfer reactions between alkenes and methylcyclohexane (to produce toluene) [6].

Whatever the contact time value, cracking is the main reaction, as expected on a medium-pore size zeolite [6,10]. Nevertheless, isomers are formed in significant amounts, together with aromatics (Fig. 5).

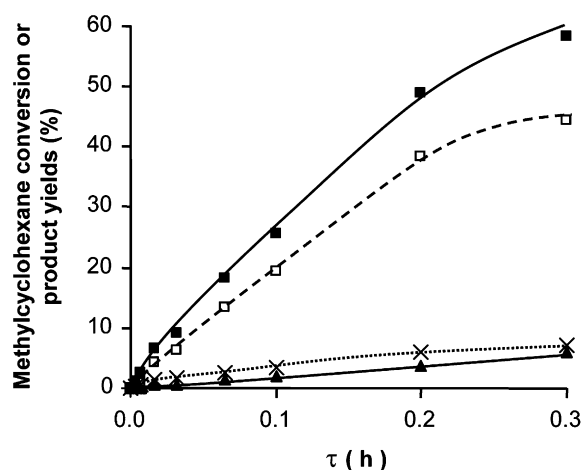


Fig. 5. Transformation of methylcyclohexane at 623 K on fresh H-EU-1 zeolite (2 min reaction). Methylcyclohexane conversion (■) and yields in cracking products (□), isomers (×) and aromatics (▲) as a function of contact time  $\tau$ .

Table 3

Molar distribution of cracking products obtained on fresh H-EU-1 zeolite (2 min reaction)

Methylcyclohexane conversion (%)	20.0	60.0
Cracking yield (%)	14.8	44.9
C <sub>1</sub>	0.23	0.17
C <sub>2</sub>	0.09	0.09
C <sub>2</sub> <sup>=</sup>	3.50	2.81
C <sub>3</sub>	17.08	19.71
C <sub>3</sub> <sup>=</sup>	4.49	1.70
iC <sub>4</sub>	35.90	40.01
nC <sub>4</sub>	6.74	7.82
iC <sub>4</sub> <sup>=</sup>	0.55	0.21
nC <sub>4</sub> <sup>=</sup>	0.56	0.22
iC <sub>5</sub>	13.72	15.11
nC <sub>5</sub>	1.10	1.23
C <sub>5</sub> <sup>=</sup>	0.52	0.22
C <sub>6</sub>	11.04	9.04
C <sub>6</sub> <sup>=</sup>	0.72	0.43
C <sub>7</sub>	2.98	1.05
C <sub>7</sub> <sup>=</sup>	1.01	0.17

Table 3 shows the distribution of cracking products obtained on fresh zeolite (2 min reaction) at two different methylcyclohexane conversions. C<sub>3</sub> and C<sub>4</sub> hydrocarbons were the main components, but the ratio of C<sub>3</sub> to C<sub>4</sub> (=0.5 at 20% conversion) was much lower than unity (as expected from the cracking of a C<sub>7</sub> hydrocarbon such as methylcyclohexane). This also was the case for the C<sub>2</sub>/C<sub>5</sub> (=0.23) and C<sub>1</sub>/C<sub>6</sub> ratios (0.02). This suggests either that a large part of the lighter compounds was not desorbed (because they were consumed in alkylation reactions involving aromatics) or that secondary formation of C<sub>4</sub>–C<sub>6</sub> hydrocarbons occurred through oligomerization/cracking of ethene and propene. Regarding the C<sub>1</sub>/C<sub>6</sub> ratio, other authors have also proposed that C<sub>6</sub> hydrocarbons can be formed through methylcyclohexane disproportionation [5]. On the other hand, the low fraction of C<sub>7</sub> hydrocarbons obtained

(4%) demonstrates, as reported previously [6,10], that desorption of these compounds was much slower than their cracking in  $C_2 + C_5$  or  $C_3 + C_4$ .

Moreover, the proportion of branched isomers in  $C_4$  and  $C_5$  products was very high; the  $i/n$  ratio for these products was equal to 6. This high value is in agreement with the higher stability of the branched carbenium ions compared with the linear ones. On the other hand, in medium-pore size zeolites, such as MFI [6,10], the shape selectivity favors diffusion, hence the desorption, of the linear isomers. Consequently, the value of the  $i/n$  ratio obtained on these zeolites is generally low (close to 1), which should also be the case on H-EU-1, which has slightly narrower pore openings than those of MFI. Therefore, the high value of the  $i/n$  ratio obtained on this zeolite could be related to the small size of this zeolite's crystallites; in this case, shape selectivity is not efficient, and the differences in diffusion rates do not play a significant role [40]. In addition, previous work on EU-1 zeolites in our laboratory has demonstrated that during ethylbenzene isomerization, the catalytic activity is due mainly to the acid sites located near or at the pore mouth [22,41], with the acid sites located inside the pores rapidly deactivated by coke. In our case, a very important contribution of the acid sites located at the pore mouth (which would be in high concentration when the crystal size is small) also could explain the non-shape-selective distribution of the cracking products. This hypothesis has also been invoked to explain the low value of the refined constraint index found for EUO zeolites [18,42,43].

Table 3 also shows that alkanes were formed in much higher amounts than alkenes; the proportion of alkanes in the desorbed cracking products was 88.4% at 20% conversion and 94.2% at 60% conversion. This suggests an important role of hydrogen-transfer reactions in global methylcyclohexane transformation. But this is in contradiction to the very low yields in aromatics obtained during the transformation, which may be explained by the retention of most of the aromatics formed in the zeolite pores. This retention could be due to a transformation of toluene (obtained from methylcyclohexane aromatization) into larger compounds ("coke") through alkylation (by alkenes, which also could contribute to the high value of the alkane/alkene ratio), followed by cyclization and/or condensation reactions. Moreover, alkenes also could be responsible for the formation of bulky aromatic compounds through oligomerization and cyclization reactions.

### 3.2.2. Effect of time on stream: Deactivation

The evolution of methylcyclohexane conversion on the H-EU-1 sample, as a function of time on stream (TOS) and for different values of contact time  $\tau$  (taken as the reciprocal of the weight hourly space velocity [WHSV]) is shown in Fig. 6a. Whatever the contact time, relatively fast and strong deactivation occurs during the first 20 min of reaction, followed by a quasi-plateau in activity. As is usually observed with zeolites, this deactivation can be related to the formation of bulky aromatic compounds (coke), which remain trapped inside the zeolite pores, leading to deactivation of the zeolite acid sites either by poisoning or by blocking the access to these sites [44].

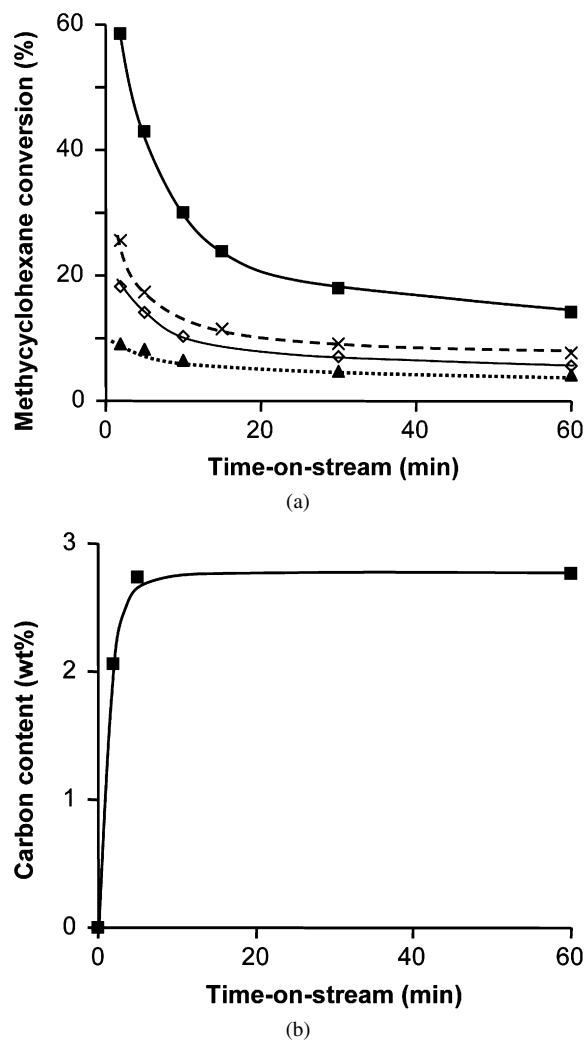


Fig. 6. Transformation of methylcyclohexane at 623 K on H-EU-1 zeolite. (a) Evolution of methylcyclohexane conversion as a function of time-on-stream, for different values of the contact time  $\tau$  (taken as the reverse of the weight hourly space velocity): (■) 0.3 h; (×) 0.1 h; (◇) 0.032 h; (△) 0.016 h. (b) Evolution of the carbon content as a function of time-on-stream for  $\tau = 0.3$  h.

Table 4

Methylcyclohexane transformation at 623 K on H-EU-1 zeolite. Total activity and activities in the formation of cracking products, isomers and aromatics obtained after 2 and 60 min of reaction

Activity ( $\text{mmol g}^{-1} \text{h}^{-1}$ )	2 min	60 min
Total	33.4	21.1
Cracking products	20.6	12.2
Isomers	10.7	7.9
Aromatics	2.1	1.0

Fig. 6b shows the increased carbon content of the zeolite as a function of TOS for a contact time of  $\tau = 0.3$  h.

Table 4 gives the total activity in methylcyclohexane transformation (estimated at  $\tau = 0$ , considering a first-order reaction in a differential reactor), along with the activities for the formation of cracking products (alkenes + alkanes), isomers and aromatics, obtained after 2 and 60 min of reaction. Deactivation (and thus coke formation) affected all reactions, and the dis-

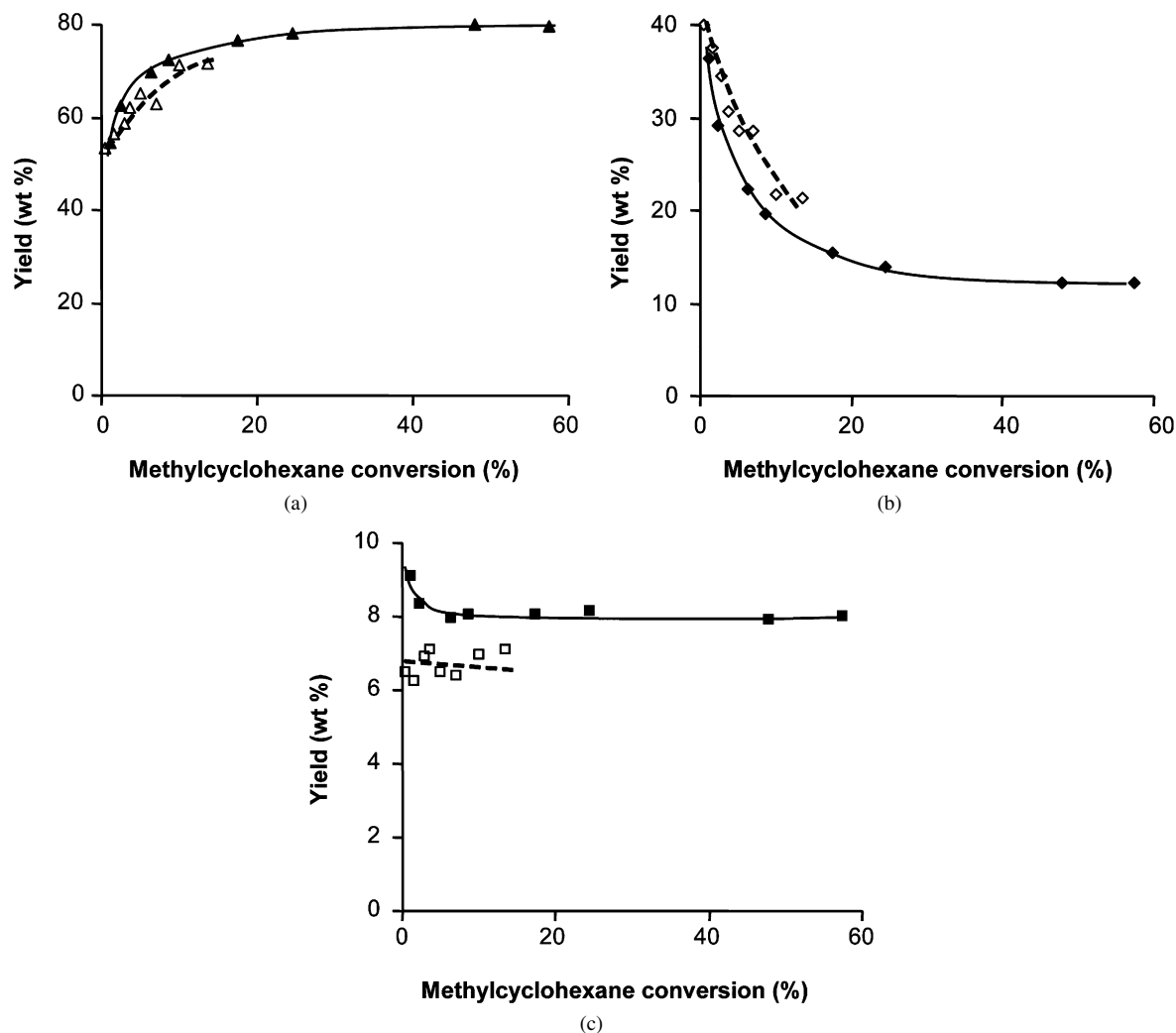


Fig. 7. Selectivity of H-EU-1 zeolite for methylcyclohexane transformation at 623 K after 2 min (fresh catalyst) and 60 min reaction (deactivated catalyst). (a) Cracking; (b) isomerization; (c) aromatization.

tribution of reactions changed slightly; the selectivity toward isomerization increased, whereas cracking and aromatization decreased, with increasing TOS (Fig. 7). This may be related to the faster deactivation (by coke formation) of the strongest acid sites, which are involved in cracking and aromatization reactions [44,45]. Differences in the locations of the reactions also could explain this change in selectivity. Cracking and aromatization, which are strongly affected by coke formation, occur inside the zeolite micropores, whereas isomerization, being less affected by coke formation, occurs either at the pore mouths or on the external surface.

Fig. 8 compares the effect of coke deposition on pore volumes and catalytic activity in the case of methylcyclohexane transformation with a contact time of  $\tau = 0.3$  h. The figure shows that coke deposition had a strong effect on micropores but a limited effect on mesopores. This indicates that coke was formed almost entirely inside the zeolite microporosity.

On the other hand, until it reached 3 wt%, coke deposition was much more detrimental to accessible micropore volume than to catalytic activity. For example, at a coke content of 2 wt%, only 20% of the micropore volume was still accessible

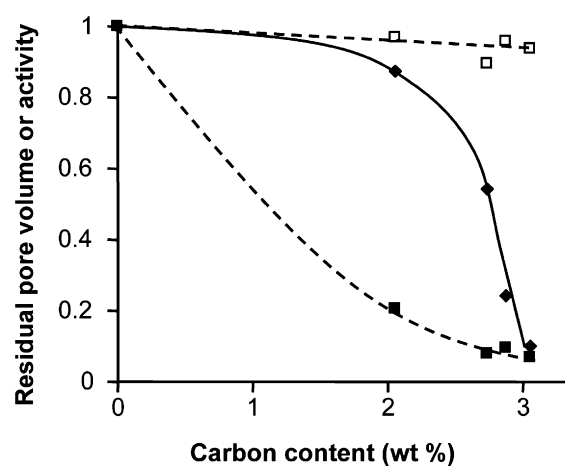


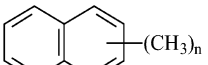
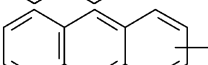
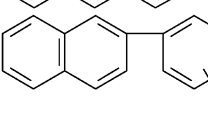
Fig. 8. Effect of coke formation (carbon content) on the activity in methylcyclohexane transformation ( $\tau = 0.3$  h) and pore volumes of H-EU-1 zeolite. (□) Mesopore + supermicropore volume; (■) micropore volume; (◆) catalytic activity. Residual values correspond to the ratio of the pore volume (or activity) for a given value of carbon content to the value at carbon content = 0.

to nitrogen at 77 K, whereas the activity had decreased by only 10% (Fig. 8). This finding is similar to that seen during ethyl-



Table 5

Composition of the “soluble coke” obtained, after different values of time-on-stream (TOS), during methylcyclohexane transformation at 623 K on H-EU-1 zeolite

TOS (min)	2	5	60	240
Carbon content (wt%)	2.10	2.70	2.80	2.95
Coke composition (wt%)				
 (CH <sub>3</sub> ) <sub>n</sub>	<i>n</i> = 3–4	100	74	78
 (CH <sub>3</sub> ) <sub>n</sub>	<i>n</i> = 1–6	0	26	22
 (CH <sub>3</sub> ) <sub>n</sub>	<i>n</i> = 3–4	0	0	ε

benzene transformation on EU-1 zeolites [22] and thus could be due to the same phenomenon: coke formation occurring inside the pores, with most of the desorbed products formed on acid sites located at the pore mouths, that is, almost unaffected by coke formation at low coke content (<3 wt% in our case). Nevertheless, the possibility of an important contribution of acid sites localized on the external surface of the zeolite crystallites cannot be excluded, although it seems unlikely that successive reactions, such as cracking and aromatization, could occur on these sites.

At 3 wt% of carbon, the situation changed; the effects of coke deposition on micropore volume and activity became similar (relative residual activity and accessible micropore volume of about 10%). This suggests that, at this stage, almost all of the sites located in the zeolite porosity, including those at the pore mouths, were deactivated by coke. Moreover, it also implies a very low (maybe even nil) contribution of external acid sites. Thus, the formation of coke can be represented in two steps: very fast formation of coke molecules on the inner acid sites (beginning with the strongest ones) during the first minutes of reaction (2 wt% of carbon after 2 min), followed by slower filling of the remaining pore volume (affecting the pore mouths).

The nature of the molecules constituting coke was determined using the method developed in our laboratory involving mineralization of the “coked” zeolite in HF solution (40%), followed by extraction of the organic compounds with a methylene chloride–*n*-pentane mixture [29,30]. This method can distinguish two kinds of coke components: one that is soluble in the organic solvent (“soluble coke”) and another that is insoluble in the organic solvent (“insoluble coke”). The composition of the former can be easily established (and quantified) by GC-MS, whereas that of the latter (which contains bulky polyaromatic hydrocarbons) can be only quantified (when found in significant quantity). In our case, only soluble coke was recovered on the low-coke content samples (<2 wt%), whereas a very small quantity of insoluble coke was found in the samples containing more than 3 wt% of carbon.

Table 5 gives the composition of the soluble coke formed during methylcyclohexane transformation at 623 K with  $\tau = 0.3$  h, for different TOS values (and thus coke content). What-

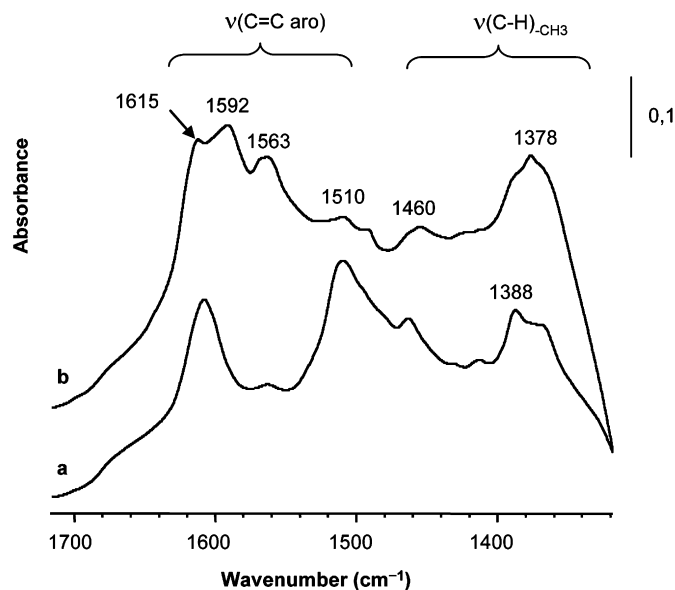


Fig. 9. IR spectra of the coked H-EU-1 samples. (a) 5 min reaction; (b) 240 min reaction. These spectra are obtained by difference between the spectrum of the coked sample and the spectrum of the “fresh” sample.

ever the TOS, methylnaphthalenes were the main products, followed by methylantracenes. A very small amount of phenyl-methylnaphthalenes also was found at TOS >60 min. The main observation is that coke composition did not change significantly with TOS, even if the IR spectra suggest the formation of small amounts of heavier polyaromatics (insoluble coke) at long TOS, that is, the appearance of bands at 1600–1590 cm<sup>-1</sup> and a decrease in the band at 1510 cm<sup>-1</sup> [46] in the IR spectrum of the sample “coked” for 240 min (Fig. 9).

The stability of the soluble coke composition with TOS indicates that the location of soluble coke molecules did not change significantly with TOS (and thus with the coke content). Thus, the strong deactivation of the zeolite observed at a carbon content >2 wt% must be due to the filling of the pore extremities by coke and deactivation of the pore mouth acid sites, as suggested earlier. In this case, the strong deactivation observed at a carbon content >2 wt% suggests that these latter sites play a very important role.

### 3.3. Role of the acid sites located at the pore mouths

To verify the role of the pore mouth acid sites, poisoning experiments were conducted adding a small amount of  $\gamma$ -collidine in the reactant (450  $\mu\text{mol h}^{-1} \text{g}_{\text{zeolite}}^{-1}$ , corresponding to 0.3 mol% in the mixture). Fig. 10 illustrates the effect of this addition on methylcyclohexane conversion for two different EU-1 samples: the H-EU-1 sample used previously and the same zeolite before protonic exchange (i.e., NaH-EU-1). This sample, obtained by simple calcination of the as-synthesized zeolite, was only partially protonic (35% of sodium, 398  $\mu\text{mol g}^{-1}$  of protonic sites).

Fig. 10 shows that the addition of collidine led to a complete deactivation of the H-EU-1 sample, suggesting that collidine not only poisoned the acid sites located on the external

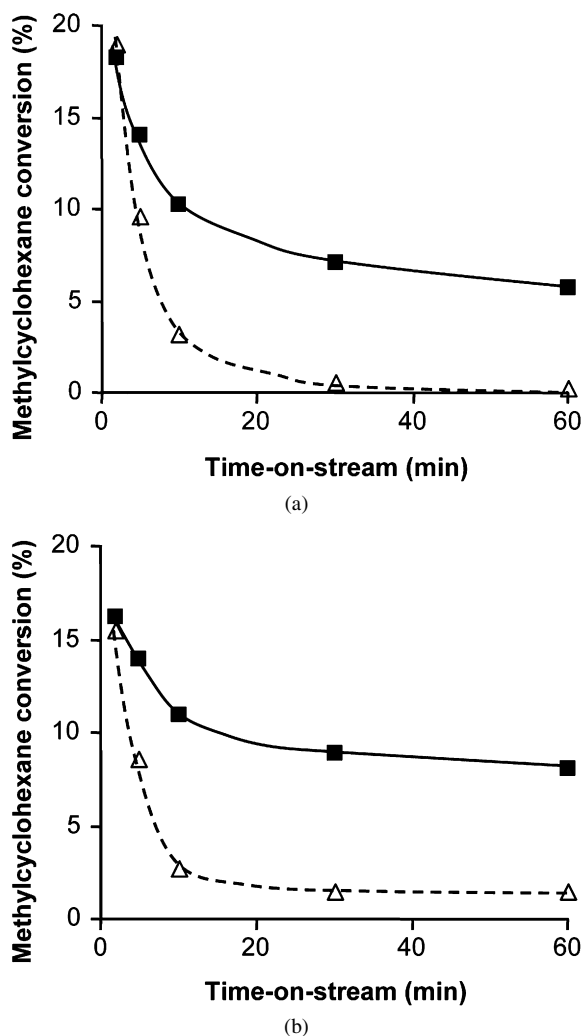


Fig. 10. Effect of collidine addition on methylcyclohexane conversion ( $\tau = 0.032$  h) on H-EU-1 (a) and NaH-EU-1 (b) zeolites. (■) Methylcyclohexane alone; ( $\Delta$ ) methylcyclohexane + collidine (0.3 mol%).

surface of the zeolite crystallites, but also blocked access to the zeolite porosity, probably by poisoning the acid sites located at the pore mouths. Previous work with collidine (or 2,4-dimethylquinoline) has shown that the amount of poison needed to obtain the maximum deactivating effect can be estimated based on the poisoning experiments, considering that during the first minutes of reaction, all of the poison molecules added are adsorbing on an acid site [47,48].

Consequently, the amount of collidine needed to obtain the maximum deactivation of the H-EU-1 sample can be estimated as  $63 \mu\text{mol g}^{-1}$ , which is not very different from the quantity of “external sites” estimated by 2,4-dimethylquinoline adsorption followed by IR spectroscopy (Table 2). Thus, it appears here that poisoning with collidine did not allow estimation of the catalytic contribution of the acid sites at the pore mouths.

On the other hand, collidine addition did not lead to complete deactivation of the NaH-EU-1 sample, even after 60 min of reaction (Fig. 10b). The amount of collidine required to obtain the maximum level of deactivation was less than that of the protonic sample ( $50 \mu\text{mol g}^{-1}$ ), suggesting that part of the

$\text{AlO}_4^-$  tetrahedrons located at the pore mouths have  $\text{Na}^+$  ions as charge-compensating cations. This observation may explain the residual activity in the case of the NaH-EU-1 poisoning; if collidine was not interacting with  $\text{Na}^+$  cations, then collidine molecules would not block some of the pore mouths, and some methylcyclohexane molecules would be able to enter the zeolite pores and react on the inner acid sites. Consequently, the residual activity, measured after 60 min of reaction, would indicate the selectivity of the inner sites: no isomer, 58% of cracking products, and 42% of aromatics.

Based on these findings, it can be suggested that all the isomers found in the reaction products were formed on the acid sites located at the pore mouths, whereas cracking products and aromatics could be formed on all of the acid sites (i.e., pore mouths and pores). This implies different selectivities for the acid sites located at the pore mouths and those located inside the pores. Moreover, the very small changes in global selectivity observed on the deactivated zeolite (Fig. 7), even with most of the micropores blocked (Fig. 8), supports the hypothesis that the catalytic contribution of the inner acid sites is very low, and thus the contribution of the acid sites located at the pore mouths is very important to methylcyclohexane transformation. This finding is in perfect agreement with earlier findings during ethylbenzene transformation on EU-1 zeolites [22], as well as with the refined constraint index of this zeolite (2.2); this value is equal to that of ZSM-12, a monodimensional 12-MR zeolite [18].

#### 4. Conclusion

In this work, methylcyclohexane transformation at 623 K was used as a model reaction to study the catalytic properties of the H-EU-1 zeolite. All of the reactions involved in methylcyclohexane transformation (i.e., cracking, isomerization, aromatization, and coking) occurred on this zeolite. As on other medium-size zeolites (MFI), cracking was the main reaction. Nevertheless, the cracking product distribution was not what was expected; branched compounds were in large excess compared with linear compounds, in contradiction to the shape-selectivity effect typically observed in medium-pore zeolites. Moreover, significant amounts of isomers were obtained, which is a common characteristic of large-pore zeolites. An important contribution of the acid sites located near the pore openings (i.e., at the pore mouths) could explain these findings.

This hypothesis is confirmed by the effect of TOS on the catalytic behavior of the H-EU-1 zeolite. Thus, although the micropores were rapidly blocked by coke, the catalytic activity remained very high until the coke content reached 3 wt%, while the selectivity remained unchanged. All of this suggests that much of the catalytic activity was due to those acid sites unaffected by coke formation, which were not located in the pores, but rather probably at the pore mouths.

Finally, the poisoning experiments with collidine confirmed the role of the acid sites located at the pore mouths. It also allowed us to distinguish the selectivity of the inner acid sites (on which only cracking products and aromatics were formed) from

that of the acid sites located at the pore mouth (on which all of the reactions occurred).

## References

- [1] A. Corma, A.V. Orchilles, *Microporous Mesoporous Mater.* 35–36 (2000) 21.
- [2] (a) C. Marcilly, *Oil Gas Sci. Tech.* 56 (2001) 499;  
(b) C. Marcilly, in: A. Galarnau, F. Di Renzo, F. Fajula, J. Védrine (Eds.), *Zeolites and Mesoporous Materials at the Dawn of the 21st Century*, in: *Stud. Surf. Sci. Catal.*, vol. 135, Elsevier, Amsterdam, 2001, p. 37.
- [3] C. Marcilly, *Acido-Basic Catalysis—Applications to Refining and Petrochemistry*, vol. 2, Technip, Paris, 2003, p. 649.
- [4] A. Corma, A. López Agudo, *React. Kinet. Catal. Lett.* 16 (1981) 253.
- [5] A. Corma, F. Mocholi, V. Orchilles, G.S. Koermer, R.J. Madon, *Appl. Catal.* 67 (1991) 307.
- [6] H.S. Cerqueira, P.C. Mihindou-Koumba, P. Magnoux, M. Guisnet, *Ind. Eng. Chem. Res.* 40 (2001) 1032.
- [7] A. Rabeharitsara, Ph.D. thesis, University of Poitiers, France, 2003.
- [8] G. Caero, P. Magnoux, J.M. Lopes, F. Ramôa Ribeiro, *Appl. Catal. A* 292 (2005) 189.
- [9] P. Magnoux, A. Rabeharitsara, H.S. Cerqueira, *Appl. Catal. A* 304 (2006) 142.
- [10] G. Caero, P. Magnoux, P. Ayrault, J.M. Lopes, F. Ramôa Ribeiro, *Chem. Eng. J.* 120 (2006) 43.
- [11] G. Caero, P. Magnoux, J.M. Lopes, F. Lemos, F. Ramôa Ribeiro, *J. Mol. Catal. A Chem.* 249 (2006) 149.
- [12] (a) J.L. Casci, J.L. Lowe, T.V. Whittam, *Eur. Pat. EP 0,042,226*, 1981;  
(b) J.L. Casci, J.L. Lowe, T.V. Whittam, *US Pat. 4,537,754*, to Imperial Chemical Industries Ltd., 1981.
- [13] Ch. Baerlocher, W.M. Meier, D.H. Olson, *Atlas of Zeolite Framework Types*, sixth ed., Elsevier, Amsterdam, 2007.
- [14] N.A. Briscoe, D.W. Johnson, M.D. Shannon, G.T. Kokotailo, L.B. McCusker, *Zeolites* 8 (1988) 74.
- [15] R. Kumar, S. Ernst, G.T. Kokotailo, J. Weitkamp, in: P.J. Grobet, W.J. Mortier, E.F. Vansant, G. Schulz-Ekloff (Eds.), *Innovation in Zeolite Materials Science*, in: *Stud. Surf. Sci. Catal.*, vol. 37, Elsevier, Amsterdam, 1988, p. 451.
- [16] G.N. Rao, R. Kumar, P. Ratnasamy, *Appl. Catal.* 49 (1989) 307.
- [17] A.R. Pradhan, A.N. Kotasthane, B.S. Rao, *Appl. Catal.* 72 (1991) 311.
- [18] W. Souverijns, L. Rombouts, J.A. Martens, P.A. Jacobs, *Microporous Mater.* 4 (1995) 123.
- [19] E. Merlen, F. Alario, S. Lacombe, E. Benazzi, J.-F. Joly, *US Pat. 6,057,486*, to Institut Français du Pétrole, 2000.
- [20] L. Rouleau, F. Kolenda, E. Merlen, F. Alario, *US Pat. 0,051,757 A1*, to Institut Français du Pétrole, 2001.
- [21] E. Merlen, F. Alario, O. Martin, N. Ferrer, S. Lacombe, L. Rouleau, J. Magne-Drisch, *US Pat. 6,514,479 B1*, to Institut Français du Pétrole, 2003.
- [22] F. Moreau, P. Moreau, N.S. Gnep, P. Magnoux, S. Lacombe, M. Guisnet, *Microporous Mesoporous Mater.* 90 (2006) 327.
- [23] J.A. Martens, W. Souverijns, W. Verrelst, R. Parton, G.F. Froment, P.A. Jacobs, *Angew. Chem. Int. Ed.* 107 (1995) 2726.
- [24] W. Souverijns, J.A. Martens, G.F. Froment, P.A. Jacobs, *J. Catal.* 174 (1998) 177.
- [25] S.J. Gregg, K.S.W. Sing, *Adsorption, Surface Area and Porosity*, second ed., Academic Press, London, 1982.
- [26] G. Leofanti, M. Padovan, G. Tozzola, B. Venturelli, *Catal. Today* 41 (1998) 207.
- [27] M. Guisnet, P. Ayrault, J. Datka, *Pol. J. Chem.* 71 (1997) 1455.
- [28] P. Ayrault, J. Datka, S. Laforge, D. Martin, M. Guisnet, *J. Phys. Chem. B* 108 (2004) 13755.
- [29] M. Guisnet, P. Magnoux, *Appl. Catal.* 54 (1989) 1.
- [30] P. Magnoux, P. Roger, C. Canaff, V. Fouche, N.S. Gnep, M. Guisnet, in: B. Delmon, G.F. Froment (Eds.), *Catalyst Deactivation*, in: *Stud. Surf. Sci. Catal.*, vol. 34, Elsevier, Amsterdam, 1987, p. 317.
- [31] K.S.W. Sing, D.H. Everett, R.A.W. Haul, L. Moscou, R.A. Pierotti, J. Rouquérol, T. Siemieniewska, *Pure Appl. Chem.* 57 (1985) 603.
- [32] J.W. Ward, in: J.A. Rabo (Ed.), *Zeolite Chemistry and Catalysis*, in: *ACS Monographs*, vol. 171, American Chemical Society, Washington, DC, 1976, p. 118.
- [33] T. Barzetti, E. Selli, D. Moscotti, L. Forni, *J. Chem. Soc. Faraday Trans.* 92 (1996) 1401.
- [34] J.P. Marques, I. Gener, P. Ayrault, J.C. Bordado, J.M. Lopes, F. Ramôa Ribeiro, M. Guisnet, *Microporous Mesoporous Mater.* 60 (2003) 251.
- [35] B.H. Chiche, F. Fajula, E. Garrone, *J. Catal.* 146 (1994) 460.
- [36] M.A. Makarova, A.E. Wilson, B.J. van Liemt, C.M.A.M. Mesters, A.W. de Winter, C. Williams, *J. Catal.* 172 (1997) 170.
- [37] O. Marie, P. Massiani, F. Thibault-Starzyk, *J. Phys. Chem. B* 108 (2004) 5073.
- [38] J.-H. Kim, A. Ishida, M. Niwa, *React. Kinet. Catal. Lett.* 67 (1999) 281.
- [39] B. Onida, L. Borello, B. Borelli, F. Geobaldo, E. Garrone, *J. Catal.* 214 (2003) 191.
- [40] P. Ratnasamy, G.P. Babu, A.J. Chandwadkar, S.B. Kulkarni, *Zeolites* 6 (1986) 98.
- [41] P. Moreau, Ph.D. thesis, University of Poitiers, France, 2005.
- [42] J.A. Martens, M. Tielen, P.A. Jacobs, J. Weitkamp, *Zeolites* 4 (1984) 98.
- [43] J.A. Martens, P.A. Jacobs, *Zeolites* 6 (1986) 334.
- [44] M. Guisnet, P. Magnoux, *Catal. Today* 36 (1997) 477.
- [45] M. Guisnet, P. Magnoux, D. Martin, in: C.H. Bartholomew, G.A. Fuentes (Eds.), *Catalyst Deactivation*, in: *Stud. Surf. Sci. Catal.*, vol. 111, Elsevier, Amsterdam, 1997, p. 1.
- [46] H.S. Cerqueira, P. Ayrault, J. Datka, M. Guisnet, *Microporous Mesoporous Mater.* 38 (2000) 197.
- [47] S. Laforge, D. Martin, M. Guisnet, *Microporous Mesoporous Mater.* 67 (2004) 235.
- [48] J. Rigoreau, S. Laforge, N.S. Gnep, M. Guisnet, *J. Catal.* 236 (2005) 45.